COMMUNICATION

Check for updates

In situ formation of an active oxygen evolution catalyst *via* photodegradation of [Ru(bpy)₃]²⁺†

Marcel Langer,[a,b] Alexander K. Mengele, [ID] [b] Riccarda Müller,[b] Julius C. Wetzel,[a] Judith Mayer,[b] Sven Rau [ID] *[b] and Carsten Streb [ID] *[a,b]

[Ru(bpy)₃]²⁺ is a widely used molecular photosensitizer (PS) for light-driven reactions in combination with separate catalysts, although the PS alone is known to promote water oxidation under aqueous conditions as well. In contrast, this behavior has not been reported for organic and aqueous solvent mixtures before. Here, we provide mechanistic insights into the role of [Ru(bpy)₃]²⁺ as PS and oxygen evolution catalyst precursor in organic media.

To date, the global energy demand is still largely met by non-sustainable energy sources.[1–3] Green hydrogen, produced by the splitting of water into its elements, is a major alternative to fossil fuels.[4,5] One approach to this end is artificial photosynthesis by using solar energy to drive the water splitting reactions, *i.e.* the oxygen evolution reaction (OER) and the hydrogen evolution reaction (HER).[6–9] Light harvesting in artificial photosynthesis is often performed by molecular photosensitizers (PS).[10–12] The metal complex [Ru(bpy)₃]²⁺ (bpy = 2,2′-bipyridine) is one of the most widely used PS species, as it combines high light absorption in the visible range (λ_{max} = 450 nm), long excited-state lifetimes and photoredox reactivity that enables both oxidative as well as reductive transformations.[13,14] [Ru(bpy)₃]²⁺ can also be deployed in various solvents, as solubility can be controlled by the choice of counter anion (*e.g.* Cl⁻ for aqueous systems, PF₆⁻ for polar organic solvents).[15,16] Thus, molecular OER and HER catalyst models can be studied both in aqueous and non-aqueous solvents, which has led to unique insights and significant progress in OER and HER catalysis.[17–22] However, it is worth noting that in aqueous systems [Ru(bpy)₃]²⁺ does not act as an innocent PS. Instead, Yoon and co-workers demonstrated that in aqueous media and in the presence of the sacrificial oxidizing agent (SOA) sodium persulfate (Na₂S₂O₈), the complex

undergoes fast, light-induced decomposition starting from the oxidized [Ru^{III}(bpy)₃]³⁺. After initial formation of an unknown intermediate, the photosystem then forms either the well-known Ru μ-oxo blue dimer water oxidation catalyst (WOC) [(bpy)₂(H₂O)RuORu(OH₂)(bpy)₂]⁴⁺ (see Fig. 1, formed at low PS concentrations) or catalytically inactive Ru μ-oxo oligomers (formed at high PS concentrations).[23] In the further course of this light-driven OER, the Ru-dimers can readily be converted by [Ru(bpy)₃]³⁺ into the fully oxidized and water oxidation-active species [(bpy)₂(O)RuORu(O)(bpy)₂]⁴⁺ (hereafter: Ru₂(v,v)).[24,25]

In contrast to this understanding of [Ru(bpy)₃]²⁺ reactivity in water, to the best of our knowledge, no similar mechanistic OER studies have been performed in predominantly organic solvents containing water. However, this is urgently required as mechanistic and catalytic studies on molecular WOCs are often performed in organic media.

Here, we report catalytic and mechanistic studies on the role of [Ru(bpy)₃]²⁺ in light-driven OER experiments in often-used acetonitrile/water mixtures and provide insights into the competing roles of [Ru(bpy)₃]²⁺ as a PS and molecular precursor of an active WOC.

The prototype OER system discussed herein consists of the PS [Ru(bpy)₃](PF₆)₂ (1 mM, PS1a) and the SOA Na₂S₂O₈ (10 mM) dissolved in a 9 : 1 (v : v) mixture of acetonitrile (MeCN) and water. The reaction conditions were adapted from previous OER studies in mixed aqueous organic solvents, see
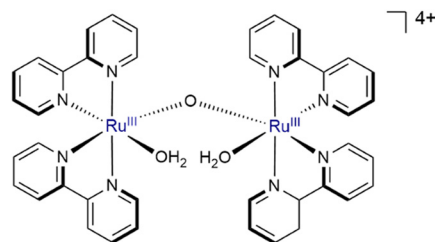
[a]Department of Chemistry, Johannes Gutenberg University Mainz, Duesbergweg 10-14, 55128 Mainz, Germany. E-mail: carsten.streb@uni-mainz.de
[b]Institute of Inorganic Chemistry I, Ulm University, Albert-Einstein-Allee 11, 89081 Ulm, Germany

Fig. 1 Structural representation of the WOC "blue dimer" *cis,cis*-[(bpy)₂(H₂O)Ru^{III}ORu^{III}(OH₂)(bpy)₂]⁴⁺ (=Ru₂(III,III)).

ESI† for details.[26] Note that in our study, the reaction solutions do not contain any WOCs. The samples were prepared under inert atmosphere, placed in a custom-built air-cooled photoreactor and irradiated with LED light (λ_{max} = 470 nm, power density: *ca.* 50 mW cm^{-2}; see ESI, Fig. S1†). Oxygen evolution was quantified *in operando*, simultaneously in solution and the gas phase using fiber-optic fluorescent sensors integrated in a sealed glass vial. For reasons of clarity and better comparison, the quantified oxygen is given in μmol. In addition, turnover numbers (TONs) and turnover frequencies (TOFs) are not calculated, as the concentration of the actual catalytically active species remains unknown.

Fig. 2 shows a representative O_2 evolution profile of the prototype OER experiment as described above. Under dark conditions (t = 0–5 min), no oxygen evolution is observed, demonstrating the integrity of the inert-atmosphere setup and the need for light to form O_2 under the given conditions (see ESI, Fig. S2†). Upon irradiation (t > 5 min) and following a short induction phase of less than 1 min, constant oxygen evolution is monitored, which is accompanied by visually detectable gas formation. After approximately 45–60 min, the amount of dissolved oxygen reaches a maximum (*ca.* 2.1 μmol, see blue curve in Fig. 2), indicating that the O_2 saturation level of the solvent mixture is reached. Diffusion into the gas phase continues, as observed by a decrease in the dissolved oxygen, while simultaneously the O_2 values in the gas phase continue to rise. The amounts of O_2 in the gas phase and in the solution, both reach a plateau after *ca.* 3–4 h, indicating the end of the OER process. A total oxygen amount of 24.1 ± 1.9 μmol was obtained, emphasizing the complete consumption of SOA as

limiting factor for sustained O_2 evolution. Persulfate is a two-electron acceptor, whereas water oxidation requires the removal of four electrons per O_2 molecule. Thus, the molar amount of $S_2O_8^{2-}$ used (50 μmol, corresponding to 10 mM) can generate 100 μmol of oxidation equivalents, which is equal to a theoretical O_2 yield of 25 μmol. This stoichiometric equivalence was further validated at different SOA concentrations (see ESI, Fig. S3†). Therefore, the O_2 quantities are within the range of measurement accuracy and identical to the number of oxidation equivalents provided by SOA.

Notably, during irradiation, the intense orange color of [Ru(bpy)$_3$]$^{2+}$ fades, indicating (partial) degradation of the PS. Depending on irradiation time and catalytic progress, the post-catalytic solutions were yellow ($t_{irradiation} \approx$ 3–10 h) or green ($t_{irradiation} \geq$ 10 h), in the latter case often accompanied by the formation of a green oily deposit (see inset photographs in Fig. 2). Note that reference experiments showed that both PS and SOA were required in the reaction system to drive this degradation and result in species capable of oxygen evolution (see ESI, Fig. S4A and B†). In addition, when [Ru(bpy)$_3$](PF$_6$)$_2$ solutions were irradiated in the absence of SOA, no color changes were observed, highlighting that the degradation is linked to a photochemical process in the presence of the SOA. This suggests that in the presence of the SOA, the PS might either undergo a persulfate-dependent oxidation to a Ru^{3+} species (with a characteristic green color), following a mechanism reported earlier by Polyansky and colleagues,[27] or a (oxidative) degradation promoted by persulfate and sulfate radical anions, as demonstrated by Bonnet and co-workers.[28] These findings are also in line with previous reports on [Ru(bpy)$_3$]$^{2+}$ degradation under aqueous conditions.[23] Note that this PS degradation can be effectively limited using dynamic irradiation conditions and reduced photon flux rates, as shown by Rau, Ziegenbalg and colleagues.[29]

In order to gain in-depth understanding of the fate of [Ru(bpy)$_3$]$^{2+}$ under irradiation, we performed *operando* UV-Vis spectroscopy under catalytic conditions (see ESI, Fig. S5 and S6†). Upon irradiation, the characteristic ^{1}MLCT (metal-to-ligand charge transfer) band of [Ru(bpy)$_3$]$^{2+}$ at 452 nm immediately loses intensity, while a new, very broad band with a concentration-dependent maximum emerges at 663 nm under prototype conditions and 672 nm under diluted conditions (by a factor of ten). Another electronic transition at 420 nm also loses intensity but becomes much more pronounced due to the occurrence of a clearly defined maximum. These features are indicative of the oxidation of [Ru(bpy)$_3$]$^{2+}$ to [Ru(bpy)$_3$]$^{3+}$, which is expected under the given reaction conditions.[30] The UV-Vis spectrum becomes very similar to the initial spectrum within a timescale of *ca.* 30–45 min, which could indicate the formation of the orange Ru$_2$(III,IV) dimer (*vide infra*).[23] Interestingly, the formation of a blue-shifted broad signal at 653 nm after 3 h might be assigned to the conversion of [Ru(bpy)$_3$]$^{2+}$ into "blue dimer" type species with different Ru oxidation states.[23] However, this conversion can only be observed under concentrated PS conditions. Alternatively, the broad band in the *operando* UV-Vis spectrum
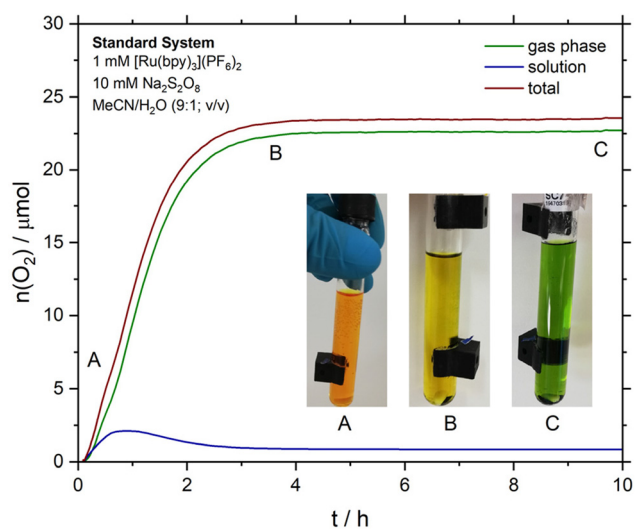

Fig. 2 Light-driven oxygen evolution profile in the gas phase (green curve), in solution (blue curve) and in total (red curve) of the OER system studied. Conditions: [Ru(bpy)$_3$](PF$_6$)$_2$ (PS1a; 1 mM), Na$_2$S$_2$O$_8$ (10 mM), solvent: MeCN/H$_2$O (9 : 1; v/v; 5 mL), LED light (λ_{max} = 470 nm; power density: *ca.* 50 mW cm^{-2}). Inset photographs show the pre- and post-catalytic reaction solutions in dependence of the irradiation time: (A): intense orange (t = 0 h), (B): yellow ($t \approx$ 3–10 h) and (C) green, often accompanied by an oily deposit ($t \geq$ 10 h).

assigned to $[Ru(bpy)_3]^{3+}$ accumulates very rapidly once light irradiation occurs and is slowly consumed by subsequent catalyst formation. At a certain point in the preceding reaction, enough catalyst has formed and no further $[Ru(bpy)_3]^{3+}$ can accumulate, as it is readily reduced to Ru(II) species by the amount of catalyst present. This interpretation is supported by the correlation of the induction phase for O_2 evolution (see Fig. 2) with the time in which the UV-Vis band at 672 nm (see ESI, Fig. S6C,† orange curve) decreases.

Moreover, the green oily deposit from a typical photo-catalytic organic OER experiment was separated by centrifugation and dissolved in water, resulting in the UV-Vis spectrum shown in the ESI Fig. S7.† The observed transitions can be assigned to two different, structurally related Ru-dimer species that form simultaneously. On the one hand, the orange Ru_2(III, IV) dimer can be identified by its characteristic MLCT transition maximum at 464 nm, while another transition maximum at 650 nm is attributed to the blue Ru_2(III,III) dimer.[23] Both dimers combine characteristic ligand-centered (LC) transitions of $\pi\pi^*_{bpy}$ at 208 nm and 288 nm, as well as an additional MLCT band at 242 nm and a very weak shoulder at 383 nm.[31] Another broad absorption in the near-IR with a maximum at 854 nm is assigned to $d\pi d\pi$ interconfigurational transitions of the blue dimer.[32] Thus, these results suggest a similar decomposition pathway of $[Ru(bpy)_3]^{2+}$ during homogeneous light-driven water oxidation using persulfate as SOA under aqueous and non-aqueous conditions, as discussed in the introduction: during the initial catalytic phase, minor concentrations of catalytically active Ru μ-oxo dimers might be formed, followed by formation of catalytically inactive Ru μ-oxo species, such as oligomers, resulting in a complex interplay between different Ru-based active and inactive species.

Further analyses showed that the type of organic solvent plays a crucial role for the observed PS conversion and its respective reactivity for the OER, as replacing MeCN with other polar organic solvents such as N,N'-dimethyl formamide (DMF) resulted in almost no O_2 evolution (ca. 0.04 μmol after 90 min corresponding to >99% less oxygen evolution compared to the prototype system in the presence of MeCN, see ESI, Fig. S8A†). Similarly, experiments in acetone yielded only extremely low O_2 quantities (ca. 0.27 μmol after 90 min corresponding to ~98.5% less O_2 evolution compared to the prototype system in the presence of MeCN, see ESI, Fig. S8B†).

Variation of the MeCN : water molar ratio also leads to major reactivity changes: the prototype system (using 9 : 1, v : v MeCN : water) yielded 23.5 μmol O_2 after 6 h irradiation, while identical experiments using 3 : 2, v : v MeCN : water gave only 4.5 μmol (corresponding to an oxygen evolution decrease of ~80%, see ESI, Fig. S8C†), indicating that solvent composition has a significant impact on PS degradation. This is substantiated by earlier reports, which suggest that light- or Ru-oxidation-induced bipyridine-to-MeCN ligand exchange is a typical degradation path for ruthenium bipyridyl photosensitizers.[33-35] Based on these considerations, we can propose a possible reaction scheme as shown in Fig. 3.
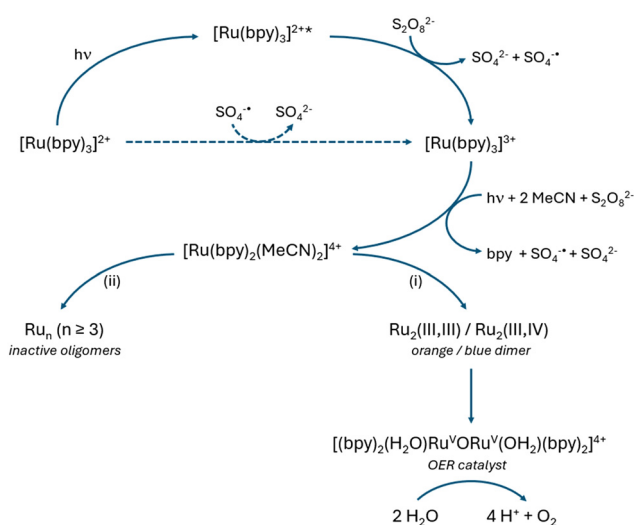

Fig. 3 Postulated reaction scheme for the formation of the active WOC of the blue dimer type using $[Ru(bpy)_3]^{2+}$ in non-aqueous MeCN solution and in the presence of $S_2O_8^{2-}$. (i) Further oxidation to OER-active dimers by $[Ru(bpy)_3]^{3+}$ or $S_2O_8^{2-}$ in the presence of a minor PS^{3+} concentration. (ii) Formation of OER-inactive Ru μ-oxo oligomers when the PS^{3+} concentration is increased. The stoichiometry has been omitted for the sake of clarity, and the water ligand could also be substituted by other ions in the solution, e.g. SO_4^{2-}, to form dimer derivatives. Adapted and modified from reference.[23,33]

To demonstrate that loss of bpy is a key factor for the $[Ru(bpy)_3]^{2+}$ degradation under the given conditions, we showed that degradation can be inhibited by the addition of free bpy ligand. Operando UV-Vis spectroscopic measurements demonstrate this effect, as no formation of the broad band around 653 nm (indicative of PS degradation) is observed (see ESI, Fig. S9†). To test this hypothesis, we performed OER experiments in the presence of additional bpy ligand using our standard photocatalytic OER setup: when an excess of bpy (100 mM) is present in solution, we observe significantly lower amounts of O_2 (max. 7.3 μmol, ~69% less oxygen compared to the prototype system, see ESI, Fig. S10†). We propose that an excess of bpy prevents the formation of significant quantities of degraded PS, thereby preventing further conversion to the catalytically active OER species.[36,37] Also note that the presence of excess bpy prevented the formation of the characteristic green oily deposit of the Ru dimers. Instead, only precipitation of colorless sodium sulfate was detected by ATR-FTIR spectroscopy (see ESI, Fig. S11†).[38] This indicates that the sulfate sources, that is persulfate, might have several functions in the given system. The primary function of persulfate is to operate as SOA. Then, the compound itself or its reaction products (e.g. strongly-oxidizing sulfate radical anions) might act as oxidants to drive the formation of the blue dimer or the oligomeric Ru μ-oxo species.

Finally, we extended our studies to various structurally related ruthenium polypyridyl PS. To this end, we investigated a selection of five additional Ru-based PS (see Fig. 4) to assess how the type of ligand impacts degradation and oxygen evol-
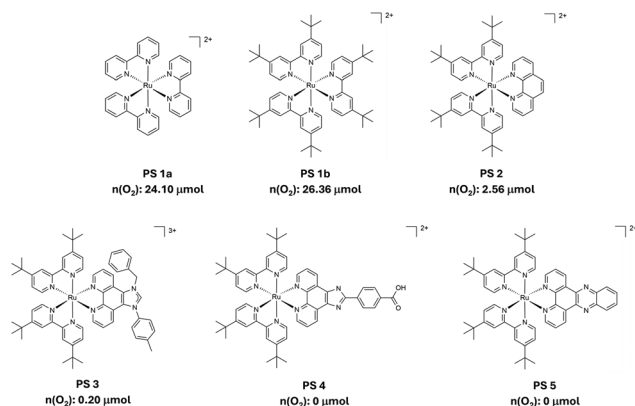
Fig. 4 Various Ru-polypyridyl PS and their maximum light-driven OER reactivity. PS1a: $[Ru(bpy)_3](PF_6)_2$; PS1b: $[Ru(tbbpy)_3](PF_6)_2$; PS2: $[Ru(tbbpy)_2(phen)](PF_6)_2$; PS3: $[Ru(tbbpy)_2(p\text{-tolbip})](PF_6)_3$; PS4: $[Ru(tbbpy)_2(ipphCOOH)](PF_6)_2$ and PS5: $[Ru(tbbpy)_2(dppz)](PF_6)_2$.

ution. All systems were tested as PS under the standard reaction conditions outlined above.

The homoleptic complex $[Ru(tbbpy)_3](PF_6)_2$ (PS1b; tbbpy = 4,4′-di-*tert*-butyl-2,2′-bipyridine) shows comparable OER activity to PS1a (*ca.* 25 μmol after 6 h of irradiation; see ESI, Fig. S12A†), whereas drastically reduced amounts of O_2 were obtained for the heteroleptic $[Ru(tbbpy)_2(phen)](PF_6)_2$ (PS2; phen = 1,10-phenanthroline; *ca.* 2.6 μmol after 3 h of irradiation; see ESI, Fig. S12B†). In contrast, no oxygen evolution was observed for the other PS $[Ru(tbbpy)_2(p\text{-tolbip})](PF_6)_3$ (PS3; *p*-tolbip = 1-(4-methylphenyl)-3-benzyl-1*H*-imidazo[4,5-*f*][1,10] phenanthroline),[39] $[Ru(tbbpy)_2(ipphCOOH)](PF_6)_2$ (PS4; ipphCOOH = 4-(1*H*-imidazol[4,5-*f*][1,10]phenanthroline-2-yl)benzoic acid),[40] and $[Ru(tbbpy)_2(dppz)](PF_6)_2$ (PS5; dppz = dipyrido[3,2-*a*:2′,3′-*c*] phenazine; for details, see ESI, Fig. S12C–E†).[41] These results suggest that the *in situ* formation of an active WOC can be effectively hindered by using heteroleptic PS, which suppress or prevent ligand exchange and Ru-dimer formation.

Conclusions

In summary, we demonstrated that in mixed aqueous/organic solvents, $[Ru(bpy)_3]^{2+}$ can undergo light-induced degradation and formation of catalytically active ruthenium dimer species capable of OER. Compared with a reference experiment performed under purely aqueous conditions, this process is notably faster when performed in organic solvent (see ESI, Fig. S22†). The catalytic system is sensitive to changes in solvent type and water content. Also, we demonstrate that structurally related Ru photosensitizer species show similar reactivity but heteroleptic complexes perform significantly worse. Thus, this report highlights that careful analysis and blank studies are required for each set of reaction conditions when using $[Ru(bpy)_3]^{2+}$ to drive photocatalysis.

Author contributions

M.L.: conceptualization, investigation, writing – original draft, project administration, methodology, data curation, data analysis; A.K.M.: investigation, formal analysis, writing – review and editing; R.M.: investigation, writing – review and editing; J.C.W.: investigation, writing – review and editing; J.M.: investigation, writing – review and editing; S.R.: resources, writing – review and editing; C.S.: conceptualization, funding acquisition, resources, supervision, writing – review and editing.

Data availability

Data for this article, including experimental spectroscopic and analytical data are available at zenodo.org at **https://doi.org/10.5281/zenodo.14760529**.

Conflicts of interest

There are no conflicts to declare.

Acknowledgements

References

1 P. J. Megia, A. J. Vizcaino, J. A. Calles and A. Carrero, *Energy Fuels*, 2021, **35**, 16403–16415.
2 S. H. Mohr, J. Wang, G. Ellem, J. Ward and D. Giurco, *Fuel*, 2015, **141**, 120–135.
3 International Energy Agency, *World Energy Outlook*, 2024.
4 S. Batool, M. Langer, S. N. Myakala, M. Heiland, D. Eder, C. Streb and A. Cherevan, *Adv. Mater.*, 2024, **36**, 2305730.
5 F. Qureshi and M. Tahir, *Int. J. Hydrogen Energy*, 2024, **69**, 760–776.
6 B. Zhang and L. Sun, *Chem. Soc. Rev.*, 2019, **48**, 2216–2264.
7 T. J. Meyer, *Acc. Chem. Res.*, 1989, **22**, 163–170.
8 Q. Wang and K. Domen, *Chem. Rev.*, 2020, **120**, 919–985.
9 J. Wang, W. Cui, Q. Liu, Z. Xing, A. M. Asiri and X. Sun, *Adv. Mater.*, 2016, **28**, 215–230.
10 L. Wang, *Catalysts*, 2022, **12**, 919.
11 D. Costabel, A. Nabiyan, A. Chettri, F. Jacobi, M. Heiland, J. Guthmuller, S. Kupfer, M. Wächtler, B. Dietzek-Ivanšić, C. Streb, F. H. Schacher and K. Peneva, *ACS Appl. Mater. Interfaces*, 2023, **15**, 20833–20842.
12 J.-H. Shon and T. S. Teets, *ACS Energy Lett.*, 2019, **4**, 558–566.
13 V. Balzani, G. Bergamini, F. Marchioni and P. Ceroni, *Coord. Chem. Rev.*, 2006, **250**, 1254–1266.

14 A. Juris, V. Balzani, F. Barigelletti, S. Campagna, P. Belser and A. von Zelewsky, *Coord. Chem. Rev.*, 1988, **84**, 85–277.

15 A. W. Adamson and J. N. Demas, *J. Am. Chem. Soc.*, 1971, **93**, 1800–1801.

16 M. Biner, H. B. Bürgi, A. Ludi and C. Röhr, *J. Am. Chem. Soc.*, 1992, **114**, 5197–5203.

17 M. P. Santoni, G. La Ganga, V. Mollica Nardo, M. Natali, F. Puntoriero, F. Scandola and S. Campagna, *J. Am. Chem. Soc.*, 2014, **136**, 8189–8192.

18 E. Deponti and M. Natali, *Dalton Trans.*, 2016, **45**, 9136–9147.

19 A. Rajagopal, F. Venter, T. Jacob, L. Petermann, S. Rau, S. Tschierlei and C. Streb, *Sustainable Energy Fuels*, 2019, **3**, 92–95.

20 Z. Huang, Z. Luo, Y. V. Geletii, J. W. Vickers, Q. Yin, D. Wu, Y. Hou, Y. Ding, J. Song, D. G. Musaev, C. L. Hill and T. Lian, *J. Am. Chem. Soc.*, 2011, **133**, 2068–2071.

21 B. Limburg, E. Bouwman and S. Bonnet, *Coord. Chem. Rev.*, 2012, **256**, 1451–1467.

22 B. Schwarz, J. Forster, M. K. Goetz, D. Yücel, C. Berger, T. Jacob and C. Streb, *Angew. Chem., Int. Ed.*, 2016, **55**, 6329–6333.

23 U. S. Akhtar, E. L. Tae, Y. S. Chun, I. C. Hwang and K. B. Yoon, *ACS Catal.*, 2016, **6**, 8361–8369.

24 J. A. Gilbert, D. S. Eggleston, W. R. Murphy, D. A. Geselowitz, S. W. Gersten, D. J. Hodgson and T. J. Meyer, *J. Am. Chem. Soc.*, 1985, **107**, 3855–3864.

25 F. Liu, J. J. Concepcion, J. W. Jurss, T. Cardolaccia, J. L. Templeton and T. J. Meyer, *Inorg. Chem.*, 2008, **47**, 1727–1752.

26 F. L. Huber, S. Amthor, B. Schwarz, B. Mizaikoff, C. Streb and S. Rau, *Sustainable Energy Fuels*, 2018, **2**, 1974–1978.

27 A. Lewandowska-Andralojc and D. E. Polyansky, *J. Phys. Chem. A*, 2013, **117**, 10311–10319.

28 B. Limburg, E. Bouwman and S. Bonnet, *ACS Catal.*, 2016, **6**, 5273–5284.

29 M. Sender, F. L. Huber, M. C. G. Moersch, D. Kowalczyk, J. Hniopek, S. Klingler, M. Schmitt, S. Kaufhold, K. Siewerth, J. Popp, B. Mizaikoff, D. Ziegenbalg and S. Rau, *ChemSusChem*, 2022, **15**, e202200708.

30 J. C. Hidalgo-Acosta, M. A. Méndez, M. D. Scanlon, H. Vrubel, V. Amstutz, W. Adamiak, M. Opallo and H. H. Girault, *Chem. Sci.*, 2015, **6**, 1761–1769.

31 T. R. Weaver, T. J. Meyer, S. A. Adeyemi, G. M. Brown, R. P. Eckberg, W. E. Hatfield, E. C. Johnson, R. W. Murray and D. Untereker, *J. Am. Chem. Soc.*, 1975, **97**, 3039–3048.

32 J. W. Jurss, J. J. Concepcion, J. M. Butler, K. M. Omberg, L. M. Baraldo, D. G. Thompson, E. L. Lebeau, B. Hornstein, J. R. Schoonover, H. Jude, J. D. Thompson, D. M. Dattelbaum, R. C. Rocha, J. L. Templeton and T. J. Meyer, *Inorg. Chem.*, 2012, **51**, 1345–1358.

33 A. Soupart, F. Alary, J. L. Heully, P. I. P. Elliott and I. M. Dixon, *Inorg. Chem.*, 2020, **59**, 14679–14695.

34 B. Durham, J. V. Caspar, J. K. Nagle and T. J. Meyer, *J. Am. Chem. Soc.*, 1982, **104**, 4803–4810.

35 A. Soupart, F. Alary, J.-L. Heully, P. I. P. Elliott and I. M. Dixon, *Coord. Chem. Rev.*, 2020, **408**, 213184.

36 T. M. McCormick, Z. Han, D. J. Weinberg, W. W. Brennessel, P. L. Holland and R. Eisenberg, *Inorg. Chem.*, 2011, **50**, 10660–10666.

37 D. Kim, D. R. Whang and S. Y. Park, *J. Am. Chem. Soc.*, 2016, **138**, 8698–8701.

38 Z. Y. Chen, D. Persson and C. Leygraf, *J. Electrochem. Soc.*, 2005, **152**, B526–B533.

39 M. Lämmle, B. Bagemihl, D. Nauroozi, L. Petermann, A. Pannwitz and S. Rau, *ChemPhotoChem*, 2022, **6**, e202200053.

40 A. Stumper, M. Lämmle, A. K. Mengele, D. Sorsche and S. Rau, *Eur. J. Inorg. Chem.*, 2018, 586–596.

41 A. K. Mengele, D. Weixler, A. Chettri, M. Maurer, F. L. Huber, G. M. Seibold, B. Dietzek, B. J. Eikmanns and S. Rau, *Chem. – Eur. J.*, 2021, **27**, 16840–16845.